RSC Advances

ROYAL SOCIETY OF CHEMISTRY

www.rsc.org/advances

Journal Name

RSCPublishing

ARTICLE

Magnetic g-C_3N_4/$NiFe_2O_4$ hybrids with enhanced photocatalytic activity

Cite this: DOI: 10.1039/x0xx00000x

Haiyan Ji[a], Xiaocui Jing[a], Yuanguo Xu[b], Jia Yan[b], Hongping Li[b], Yeping Li[b], Liying Huang[b], Qi Zhang[c], Hui Xu[*b], Huaming Li[*b]

Received 00th January 2012,
Accepted 00th January 2012

DOI: 10.1039/x0xx00000x

www.rsc.org/

Composite photocatalysts have attracted much attention in exploring both high efficient and low cost materials. In this study, novel magnetic g-C_3N_4/$NiFe_2O_4$photocatalysts were fabricated by a facile chemisorption method. X-ray diffraction (XRD), transmission electron microscopy (TEM), IR spectra (IR), UV-vis diffuse reflectance spectra (DRS) and X-ray photoelectron spectroscopy (XPS) were utilized to analyze the structure and property of samples, which indicated that $NiFe_2O_4$ had been integrated into the surface of g-C_3N_4 successfully. The as-prepared 7.5% g-C_3N_4/$NiFe_2O_4$with best photocatalytic activity can keep high photocatalytic activity and stability after five runs in the presence of hydrogen peroxide under visible light irradiation. During the catalytic reaction, the synergistic effect between g-C_3N_4 and $NiFe_2O_4$ can accelerate photogenerated charges separation and facilitate the photo-Fenton process to get an enhanced photocatalytic activity. Moreover, the collection and recycle of photocatalyst had become readily owing to the distinctive magnetism of g-C_3N_4/$NiFe_2O_4$.

Keywords: g-C_3N_4/$NiFe_2O_4$, photocatalytic degradation, magnetism

Introduction,

In the last decades, the term "photocatalyst" has become prevalent like "nano" in the field of environmental chemistry due to photocatalytic materials' conspicuous functions. Degradation of contaminants, redox of organic chemicals and production of hydrogen, even molecule or ion detection can be achieved by photocatalysts under UV-visible light irradiation.[1-4] Nevertheless, most of photocatalysts are faced with one problem: difficult recycling process and constantlysecondary pollution on the environment. Recently, the development of magnetic photocatalyst has interested a multitude of researchers,especiallyfor MFe_2O_4 (M=divalent metal ion, e.g. Zn, Ni, Co, Cu, etc.) materials due to their easily recycling. Nanocrystalline ferrites, typical representatives of magnetic materials with high magnetic permeability and electrical resistivity have several distinctive applications for material science such as drug carrier, medical diagnostics, information storage, position sensing, spintronic devices.[5,6] Nickel ferrite is one kind of inverse spinel with the chemical formula AB_2O_4 in which equal number of Ni^{2+} and Fe^{3+} reside on octahedral sites and remaining Fe^{3+} reside on tetrahedral sites. The band gap energy of $NiFe_2O_4$ is ~2.19 eV,[7] however, there is still a standing controversy on it regardless of experimental data or computational results.[8-10] Unfortunately, pure $NiFe_2O_4$alwaysshows weak photocatalytic activity even though in Fenton reaction, so somecontributionshave been made to improve the photocatalysis.Combination with other semiconductor materials and dopingwith lanthanide elements have been verified meaningful to solve the problem. Rana synthesized the anatase TiO_2-coated $NiFe_2O_4$ through reverse micelle and hydrolysis to degrade methyl-orange dye and inactivate bacteria.[11] When Ni ferritewas substituted by neodymium,absorption edge red shifted and band gapnarrowed, which inducedsignificantly enhanced photoactivity.[12] In recent years, Wang and Fu synthesized $NiFe_2O_4$/MWCNT to degrade phenol, p-nitrophenol (PNP) with C/C_0 reaching 90% in 400 min under UV light.[13] Later, they prepared $NiFe_2O_4$-graphene hybrids with outstandingphotodegradationbehaviour which may benefit from the well electroconductivity of graphene prolonging the life of photoinduced carriers.[14] Therefore, fabricating a composite photocatalyst to enhance the photocatalytic activity of $NiFe_2O_4$ can be a feasible and efficient approach.

As a class of novel organic semiconductor, graphitic carbon nitride (g-C_3N_4) has prominent optical and photoelectrochemical properties with band gap ~2.7 eV.[15] It has been reported that g-C_3N_4can split water for hydrogen production and degrade organic pollutants under visible light irradation.[16-17] Besides, a great deal of research has confirmed that coupling g-C_3N_4 with noble metal, composite oxide, metal oxide and metal-free material could achieve exceptionally high photocatalytic capability. Normally the enhanced photocatalytic activity of semiconductor composite are attributed to the synergistic effect of heterojunction structure, like the combination of g-C_3N_4 and Bi_2WO_6,[18] WO_3,[19,20] ZnO,[21] $BiPO_4$,[22] $BiVO_4$,[23] CdS[24] and BiOX (X=Cl, Br, and I) etc.[25,26] The matching energy level between g-C_3N_4 and another semiconductor can improve the separation and immigration rate of photoinduced electron-hole pairs. Lately, g-C_3N_4/$ZnFe_2O_4$ exhibiting superior photocatalytic activity has been reported for hydrogen generation and aqueous organic pollutants degradation.[27-29]Butg-C_3N_4/$NiFe_2O_4$ has not been studied till now, so we concentrate on the work hoping to construct one typical easily recycled materialandmeanwhile improve the photocatalytic performance of $NiFe_2O_4$.

Herein, we fabricated g-C_3N_4/$NiFe_2O_4$ hybrid material to build a semiconductor-semiconductor heterojunction via a convenient chemisorption method which has many advantages: availability of instruments, simplicity of operation and safety of procedure.[30]The crystal structure, surface characteristic, optical and magnetic property of g-C_3N_4/$NiFe_2O_4$ products had been characterized by XRD, TEM, DRS and VSM respectively. Methylene blue (MB) was selected as a target pollutant to investigate the photocatalytic activity of g-C_3N_4/$NiFe_2O_4$ composite with different content of g-C_3N_4. The degradation rate of MB can reach 87% in 4 h for the optimum ratio 7.5% g-C_3N_4/$NiFe_2O_4$and more g-C_3N_4 (10%) would cause a decreasing activity under visible light irradiation. In the section of mechanism, the energy band matching of g-C_3N_4/$NiFe_2O_4$heterojunction and the driving force of photocatalytic degradation for MB were discussed.

Experimental

2.1 Synthesis of $NiFe_2O_4$

All reagents were of analytical grade and were used without further purification. At first, 1 mmol $Fe(NO_3)_3$•$9H_2O$ and 0.5 mmol $Ni(NO_3)_2$•$6H_2O$ was added into 17 mL absolute ethanol in a 20 mL Teflon-lined autoclave and magnetically stirred for 30 min at room temperature. Secondly, the reddish brown emulsion was precipitated and adjusted to a pH of 13 by adding 6 M NaOH solutiondropwise. Thirdly, the precursor was sealed in a stainless steel tankand heated at 180 □ for 20 h after stirring for another 30 min. When the reaction terminated, the product was cooled down at room temperature and washed three times by water and ethanol separately, and then dried at 60 □ for later use.

2.2 Synthesis of g-C_3N_4/$NiFe_2O_4$ composites

The preparation of g-C_3N_4 is according to the method from our previouswork.[31]The g-C_3N_4/$NiFe_2O_4$ products with varying g-C_3N_4 content were synthesized in the following process: 120 mg $NiFe_2O_4$and g-C_3N_4 (mass fraction of g-C_3N_4: 5, 7.5, 10 wt%) were added into a beaker containing 20 mL absolute ethanol and kept magnetically stirring for 10 h at room temperature; then the obtained suspension was put in a 100 □ drying oven for 12 h without other operations. The obtained products are labeled as 5% g-C_3N_4/$NiFe_2O_4$, 7.5% g-C_3N_4/$NiFe_2O_4$ and 10% g-C_3N_4/$NiFe_2O_4$.

2.3 Characterization

XRD patterns of the samples were obtained on the X-ray diffractometer (Bruker D8) with Cu Kα radiation (λ=1.5418 Å) in the range of 2θ=10-80°. Transmission electron microscopy (TEM) micrographs were taken with a JEOL-JEM-2010 (JEOL, Japan) operated at 200 kV. The UV-vis diffuse reflectance spectra (DRS) of the samples were obtained on a UV-vis spectrophotometer (UV-2450, Shimadzu Corporation, Japan) using $BaSO_4$ as the reference.Infrared (IR) spectra of all the catalysts (KBr pellets) were recorded on the Nicolet Model Nexus 470 IR equipment. Elemental compositions were detected by X-ray photoelectron spectroscopy (XPS) analysis, which was performed on an ESCALab MKII X-ray photoelectron spectrometer using the Mg Kα radiation. The magnetic property of $NiFe_2O_4$ and g-C_3N_4/$NiFe_2O_4$ composites was measured in a vibrating sample magnetometer (VSM) (Quantum Design Corporation, USA) with a maximum applied field of ± 2 T at 300 K.

2.4 Photocatalytic activity measurement

The MB degradation experiment was performed to evaluate the photocatalytic activity of samples under a 300 W Xe lamp with a 400 nm cutoff filter. 0.05 g photocatalysts were added into 50 mL MB (10 mg/L) in a Pyrex photocatalytic reactor connected to a circulating water system which could keep the reaction temperature at 30 □. In addition, continuous aeration was pumped to provide the reaction with oxygen and mix the suspension as well. Prior to irradiation, dark reaction accompanied by magnetic stirring for 1h was necessary to reach absorption-desorption equilibrium between the photocatalyst and MB solution. During irradiation, 4 mL suspension was taken at defined time intervals. Then the sample was tested with a UV-vis spectrophotometer (UV-2450, Shimadzu) after centrifuge at the wavelength of 664nm which is the maximal absorption band of MB. In the H_2O_2 system, 1 mLH_2O_2 was injected into the reaction suspension as soon as the Xe lamp was turned on. Meanwhile the sampled specimen must be tested in time.

Results and discussion

3.1 XRD analysis

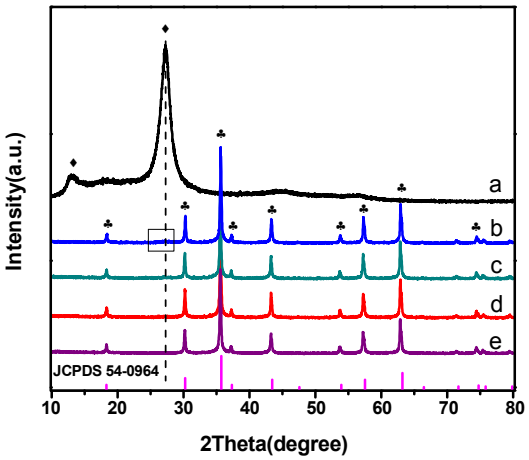

Fig. 1 XRD patterns of (a) g-C_3N_4, (b) 10% g-C_3N_4/$NiFe_2O_4$, (c) 7.5% g-C_3N_4/$NiFe_2O_4$, (d) 5% g-C_3N_4/$NiFe_2O_4$, (e) $NiFe_2O_4$.

Fig. 1 displays the XRD patterns of samples and all of the peaks have been marked with two kinds of symbols (♦ for g-C_3N_4 and ♣ for $NiFe_2O_4$). As shown in Fig. 1, the diffraction peaks at18.4°, 30.3°, 35.7°, 37.3°, 43.3°, 53.8°, 57.3°, 63.0° and 74.5°were matching well with (111), (220), (311), (222), (400), (422), (511), (440) and (533) crystalline planes of $NiFe_2O_4$ respectively (JCPDS 54-0964). It was noteworthy that there was no peak of impurity for samples b, c, d and e, which proved pH=13 can hinder the formation of Fe_2O_3. Besides, the peaks at 27.4° and 13°can be indexed as (002), (100) diffraction plane of g-C_3N_4, respectively.[32]Obviously no peak shift occurred for $NiFe_2O_4$, so the chemisorption process did not have an influence on the crystal structure. More importantly, when the content of g-C_3N_4 increased to 10%, the peak at 27.4° appeared while for other proportions the peak was not observed because of the low g-C_3N_4 content.

3.2 TEM analysis

In order to figure out the origin of activity changes before and after $NiFe_2O_4$ combined with g-C_3N_4, the particle size and morphology of catalysts were investigated by means of TEM. In Fig. 2(a), it can be clearly observed that $NiFe_2O_4$ had two totally different types of grain morphologies: the large polygon

plates (about 100nm) and the nanoscale particles (about 8 nm). So, the crystallite size distraction of $NiFe_2O_4$ could be properly bimodal.[33,34] Fig. 2(b) illustrated that $NiFe_2O_4$ polygon plates and nanoparticles adhered to the g-C_3N_4 flake and the dispersion of $NiFe_2O_4$ nanoparticles was better than that of pure $NiFe_2O_4$, which would be beneficial to form the heterojunction structure and promote the separation efficiency of photoinducedcarriers.

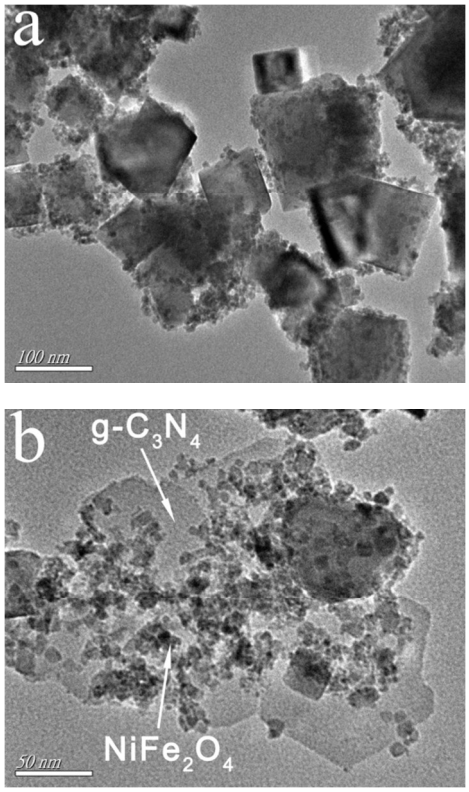

Fig. 2 TEM images of (a) $NiFe_2O_4$, (b) 7.5% g-C_3N_4/$NiFe_2O_4$.

3.3 IR analysis

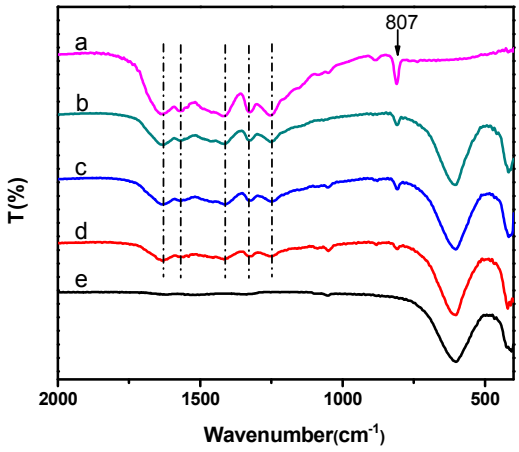

Fig. 3 IR spectra of(a) g-C_3N_4, (b) 10% g-C_3N_4/$NiFe_2O_4$, (c) 7.5% g-C_3N_4/$NiFe_2O_4$, (d) 5% g-C_3N_4/$NiFe_2O_4$, (e) $NiFe_2O_4$.

The IR spectrum enables us to distinguish molecular structure of g-C_3N_4 from other organic chemicals easily and sensitively. In Fig. 3, g-C_3N_4 and g-C_3N_4/$NiFe_2O_4$samples all had a group of absorption peaks in the 1200-1650 cm^{-1} region, corresponding to the stretching vibration modes of C=N and C–N heterocycles and the peak at 807 cm^{-1} to the breathing mode of triazine units.[35,36] Additionally the strong absorption peak at 608 and 417 cm^{-1} can be ascribed to the stretching vibrations of Fe–O bonds in tetrahedral positions and Metal–O bonds in octahedral positions respectively.[37,38]Moreover, as the mass fraction of g-C_3N_4 increased from 5% to 10% the peak at 807 cm^{-1} appeared and became sharp gradually which demonstrated g-C_3N_4 and $NiFe_2O_4$ have been integrated together.

3.4 XPS

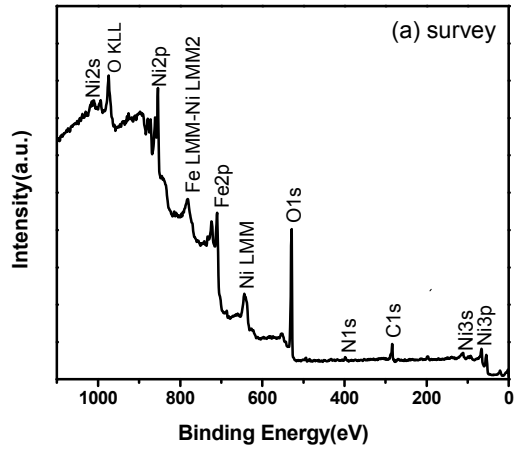

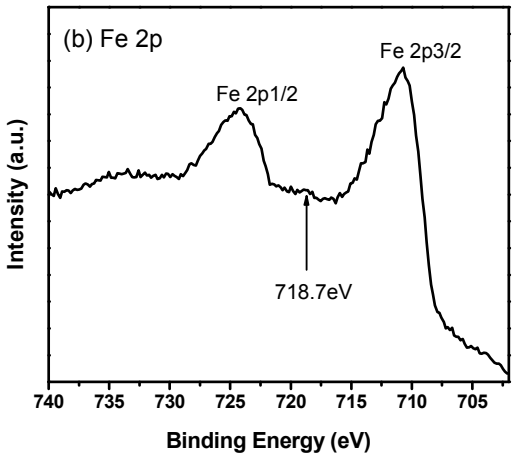

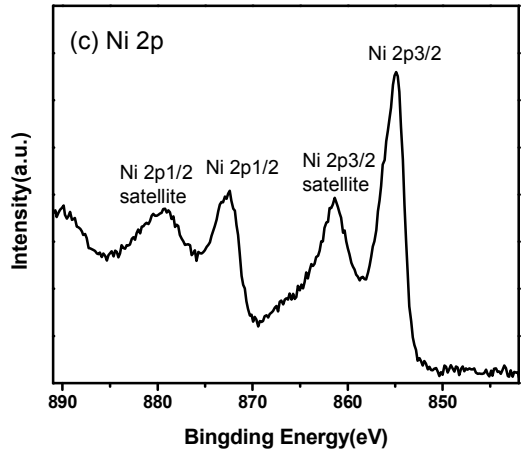

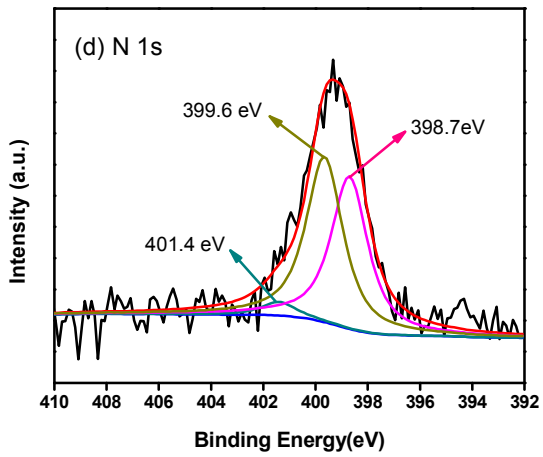

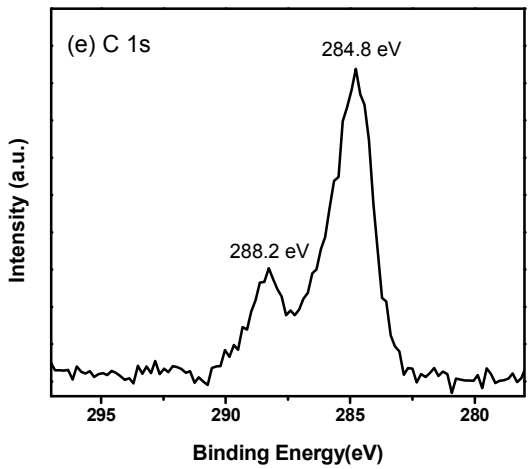

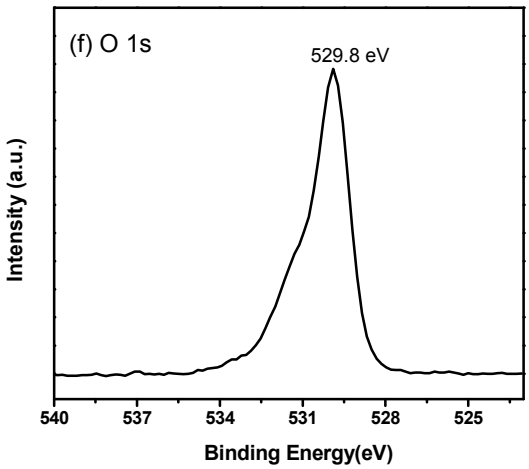

Fig. 4 XPS spectra of 7.5% g-C_3N_4/$NiFe_2O_4$ hybrid material (a) survey of the sample, (b) Fe 2p, (c) Ni 2p, (d) N 1s, (e) C 1s, (f) O 1s.

Fig. 4 is the XPS spectra of 7.5% g-C_3N_4/$NiFe_2O_4$.The survey spectrum was illustratedin Fig. 4(a), clarifyingthat g-C_3N_4/$NiFe_2O_4$ surface consisted of Fe, Ni, N, C and O elements. The typical high resolution XPS spectra of Ni 2p (Fig. 4(c)) and O 1s (Fig. 4(f)) were consistent with those reported in previous literature.[14]It was also feasible to derive information regarding Fe oxidation states from the satellite features of Fe2p. In Fig. 4(b) the binding energy of Fe 2p3/2 was observed at 710.7 eV rather than 711.2 eV but the satellite peak (718.7eV) at 8.0eV above the principal peak could be found. Thus the presence of Fe^{2+} can be ruled out.[39,40] In Fig. 4(d) the N1s peak at ~399 eV was wide and could be fit into three peaks which were 401.4, 398.7 and 399.6 eVcorresponding to C−N−H, C═N−C and N−$(C)_3$ functional groups of g-C_3N_4 respectively. Compared with peak at 400.1 eV in the reported literature, the peak shifted 0.5 eV to 399.6 eV, implying that the chemical environment of N atoms in N−$(C)_3$ groups has changed.[41]Since XPS is a surface analytical tool, the surface chemical shift happens when the local bonding environment of a species is affected. As shown in Fig. 4(e) the C1s had two obvious peaks at 284.8 and288.2 eV, the former could be ascribed to carbon absorbed casually on the surface of g-C_3N_4 and the latter can be attributed to sp^2 hybridized C (N−C═N).[42] The data of XPS further confirmed the coexistence of g-C_3N_4 and $NiFe_2O_4$, which was in agreement with the results of XRD and IR analysis.

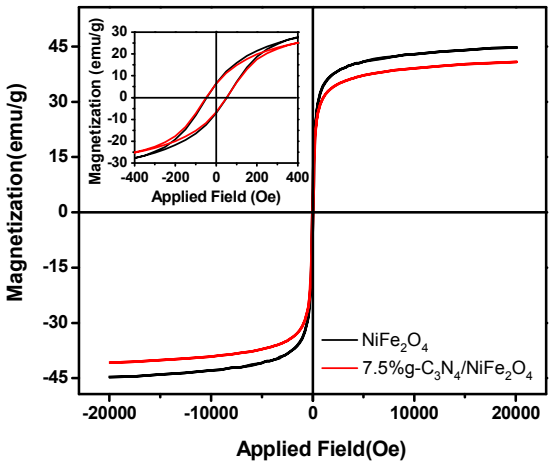

Fig. 5 Magnetization curves of the photocatalysts.

3.5 Magnetic property

When this photocatalytic material was designed, its magnetic characteristic attracted us from beginning to end. Fig. 5 illustrates magnetization curves of pure $NiFe_2O_4$ and 7.5% g-C_3N_4/$NiFe_2O_4$: X-axis represents the applied magnetic field *H* and Y-axis represents magnetization*M*. It could be estimated that the saturation magnetization M_s of $NiFe_2O_4$ and 7.5% g-C_3N_4/$NiFe_2O_4$ was about 45 and 40 emu/g respectively and the coercivityH_c was around 50 Oe without much difference between two samples in the insert figure. The presence of low-content g-C_3N_4less influenced the composite magnetism so that the collection and recycle of photocatalyst could be readily available by the external magnet. The photo in Fig. 7(b) exhibited the separation of 7.5% g-C_3N_4/$NiFe_2O_4$photocatalystfrom the reaction system after the fifth recycle of MB degradation.

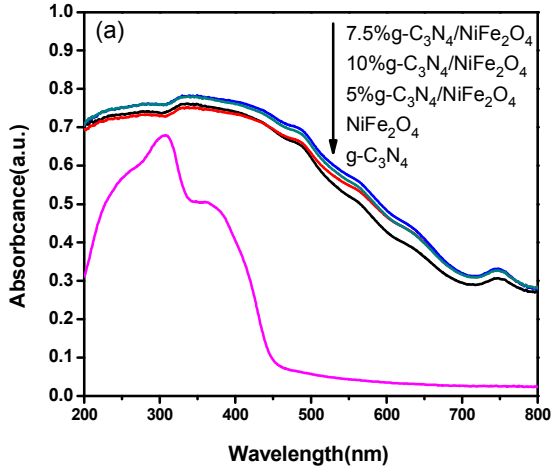

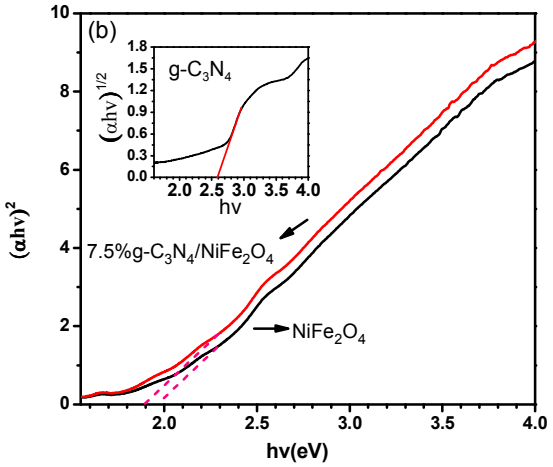

Fig. 6(a) UV-vis diffuse reflectance spectra, (b) $(\alpha h\nu)^2$ versus hν curves of $NiFe_2O_4$ and 7.5% g-C_3N_4/$NiFe_2O_4$.

3.6 UV-visanalyses

In Fig. 6(a) the UV-vis diffuse reflectance spectra reflected the samples' optical properties: g-C_3N_4 had an absorption edge around 460nm while $NiFe_2O_4$ and its composites had much stronger, wider absorption in the visible region. The distinct band gap, molecular structure and color of catalysts were considered to explain the difference in absorption range and intensity. It was also noted that 7.5% g-C_3N_4/$NiFe_2O_4$ composite had the strongest absorption intensity, which suggested that the integration of g-C_3N_4 and$NiFe_2O_4$could promote the photoabsorption ability.[43] Commonly a classic Tauc plot is carried out to estimate the amorphous semiconductor's band gap energy according to the relation: $(\alpha h\nu)^n$ versus hν. In Fig. 6(b) the results indicated that $NiFe_2O_4$ was one direct band gap semiconductor and E_g of g-C_3N_4 and$NiFe_2O_4$ was about 1.98 and1.9 eV respectively. The narrowed band gap of g-C_3N_4/$NiFe_2O_4$ would reinforce the visible light absorption intensity. Besides, the illustration in the upper left demonstrated g-C_3N_4 was an indirect transition and itsband gap energy was around 2.6eV close to the reported paper.[23]

4.1 Photocatalytic decomposition of MB

Fig. 7(a) shows the MB degradation curves with varying catalysts under visiblelight illumination. It can be seen that after 4 h of visible light irradiation the proportion C/C_0reached 57%, 66%, 87% and 76% for $NiFe_2O_4$, 5% g-C_3N_4/$NiFe_2O_4$, 7.5% g-C_3N_4/$NiFe_2O_4$ and 10% g-C_3N_4/$NiFe_2O_4$ with H_2O_2 respectively. The result clearly revealed that 7.5% g-C_3N_4/$NiFe_2O_4$ exhibited the best photocatalytic performance with H_2O_2 and thephotocatalytic degradation efficiency of MB forpure $NiFe_2O_4$was no more than 10% when there was no H_2O_2. Thereby it can be concluded that the obtained $NiFe_2O_4$ and g-C_3N_4/$NiFe_2O_4$ can effectively activate H_2O_2along with the visible light illumination. Furthermore the activation can be enhanced by the heterojunction structure. Besides, the best photocatalytic performance for 7.5% g-C_3N_4/$NiFe_2O_4$ can be attributed to the proper adsorption of MB and the enough active sites on the photocatalystsurface.In Fig. 7(b)MB degradation for the mechanically mixed sample was 65% lower than 7.5% g-C_3N_4/$NiFe_2O_4$composite, which directly verified the successful combination of g-C_3N_4 and $NiFe_2O_4$. At the same time the rate of photocatalytic reaction was also studied by fitting the zero order kinetic (C_0−C=kt) and the results were

displayed in Fig. 7(c) and Table. 1. The photodegradation rate of 7.5% g-C_3N_4/$NiFe_2O_4$ under visible light irradiation was 1.5 times higher than those of pure $NiFe_2O_4$. To further study the recyclability of g-C_3N_4/$NiFe_2O_4$ composite, five runs of photodegradation experiment were carried out. As can be seen in Fig. 7(d), g-C_3N_4/$NiFe_2O_4$photocatalystcould keep unequivocally high photocatalytic activity after five repeating useso the heterojunction structure was stable.

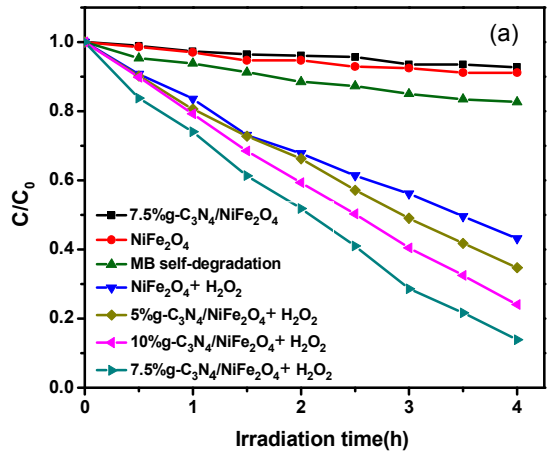

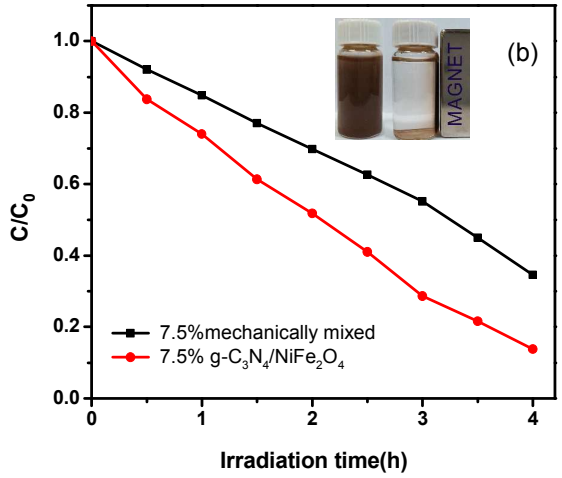

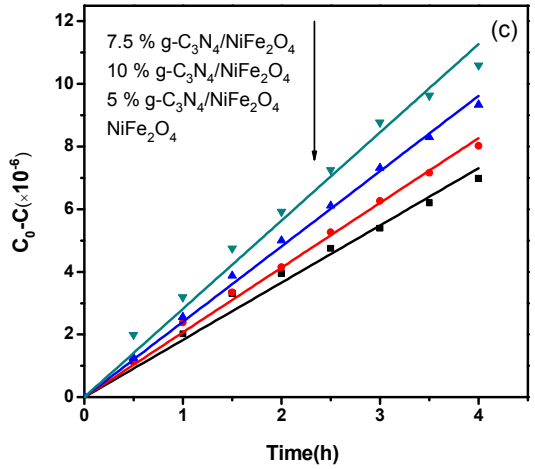

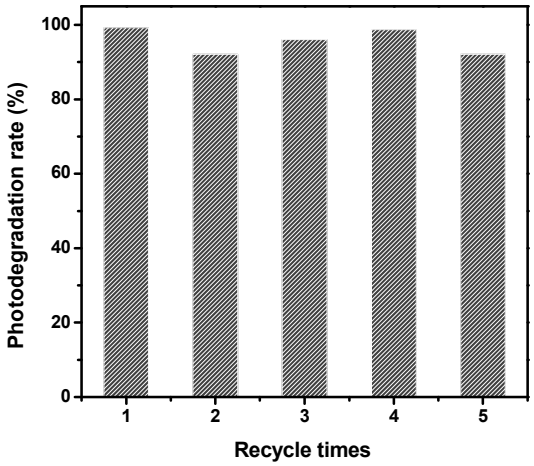

Fig. 7 (a)Photocatalytic performance of samples, (b) activity comparison between 7.5% g-C_3N_4/$NiFe_2O_4$ and 7.5% mechanically mixed, (c) kinetic fit diagram, (d)cycling runs of 7.5% g-C_3N_4/$NiFe_2O_4$photocatalystfor MB degradation.

Table. 1 Zero-order kinetic constant for MB degradation with different photocatalyst.

Samples	$k(1\times10^{-6}\text{mol}\cdot\text{L}^{-1}\cdot\text{h}^{-1})$	R^2
$NiFe_2O_4$	1.83	0.9954
5% g-C_3N_4/$NiFe_2O_4$	2.07	0.9986
10% g-C_3N_4/$NiFe_2O_4$	2.40	0.9990
7.5% g-C_3N_4/$NiFe_2O_4$	2.82	0.9958

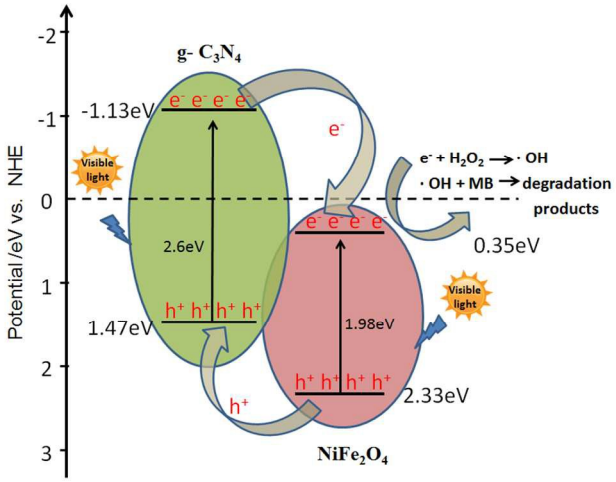

Fig. 8 Heterojunction diagram for electrons transfer in g-C_3N_4/$NiFe_2O_4$ composite.

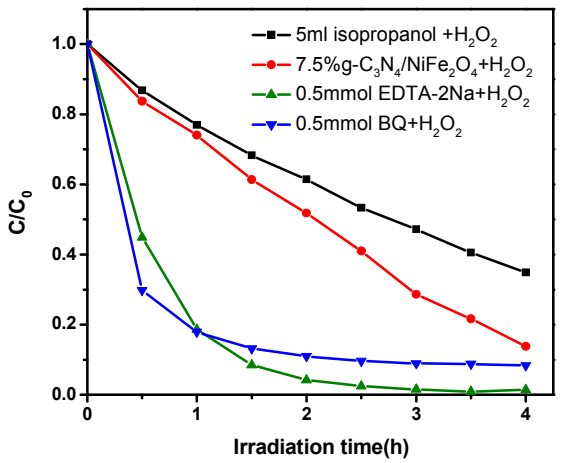

Fig. 9 Photocatalytic performance of 7.5% g-C_3N_4/$NiFe_2O_4$ with different scavengers for MB degradation.

5 Photocatalytic mechanism discussions

As mentioned above MB photodegradation capability has been improved by the heterojunction structure in the interfacial of g-C_3N_4/$NiFe_2O_4$ composite. Then we calculated $NiFe_2O_4$'s conduction band E_{CB}= 0.35 eV and E_{VB} = 2.33eVaccording to equation(1) where X is semiconductor's electronegativity and E_c is the energy of free electron on the hydrogen scale.[32] On the basis of experimental data, the scheme of a possiblephotocatalytic mechanism is presented in Fig. 8. Firstly, electrons on the VB position were excited to the CB position for both g-C_3N_4 and$NiFe_2O_4$ under visible light irradiation. Secondly, electrons on the CB of g-C_3N_4moved to the CB of $NiFe_2O_4$ and holes on the VB of $NiFe_2O_4$ transferred to the VB of g-C_3N_4. As a result, the redistribution of electrons and holes preventedphotoinduced carriers from recombination quickly. On the other hand, the CB value of $NiFe_2O_4$ (0.35eV) is less negative than $E^0(O_2/\bullet O_2^-)$ (−0.046 eVvs NHE),[44] so O_2 would not be reduced by electrons to generate $\bullet O^{2-}$ on the photocatalyst surface. Additionally, compared with the $E^0(\bullet OH/OH^-)$ (2.38 eVvs NHE),[45] the VB potential of g-C_3N_4 (1.47eV) is less positive, which implied that •OH would not be yielded by the oxidation of OH^- with holes.

For the purpose of confirming the main active species, trapping experiments were carried out and isopropanol, 1,4-benzoquinone(BQ) and disodiumethylenediaminetetraacetate (EDTA-2Na) was added to capture hydroxyl radical (•OH), superoxide radical ($\bullet O_2^-$) and hole (h^+) respectively. It can be clearly observed in Fig. 9 that the addition of 5 mLisopropanol caused the suppression of MB degradation rate while the addition of 0.5 mmolEDTA-2Na and BQ improved the degradation activity of MB. The results may reveal that the main active species should be •OH instead of $\bullet O_2^-$ and h^+, which is in agreement with the hypothesis of photocatalyticmechanism diagram above. Additionally Wang analyzed the photo-Fenton reaction routes and proved that •OH played an vital role in the oxidation process of benzene to phenol for $FeCl_3$/mpg-C_3N_4hybrids.[46]There are related studies supporting the trapping experiment and mechanism research as well.[47,48]

In Fenton and photo-Fenton reaction, iron-based species can generate highly reactive hydroxyl radicals (•OH) to treat a large variety of water pollutants. Owing to the quick conversion from Fe^{3+} into Fe^{2+}, the degradation activityin photo-Fenton reaction becomes many times higher than the classical Fenton reaction under visible light illumination.[28,49]Here the photocatalytic process and photo-Fenton reaction both function: electrons and holes transfer to opposite direction under visible light irradiation; electrons on CB of $NiFe_2O_4$ can react with H_2O_2 and Fe^{3+} to produce $\bullet OH$ for the oxidation of MB, the photodegradation reaction can be expressed as follows:

$$E_{CB} = X - E_c - \frac{1}{2}E_g \quad (1)$$

$$Fe^{2+} + H_2O_2 \longrightarrow Fe^{3+} + \bullet OH + OH^- \quad (2)$$

$$Fe^{3+} + H_2O_2 \xrightarrow{h\nu} Fe^{2+} + \bullet OH + H^+ \quad (3)$$

$$Fe^{3+} + e^- \longrightarrow Fe^{2+} \quad (4)$$

$$H_2O_2 + e^- \bullet \longrightarrow OH + OH^- \quad (5)$$

$$\bullet OH + MB \longrightarrow \text{degradation products} \quad (6)$$

Conclusions

In conclusion a simple chemisorption technique was applied to fabricate the magnetic g-C_3N_4/$NiFe_2O_4$ for MB degradation.With a matching energy band, g-C_3N_4/$NiFe_2O_4$ possessed favorable optical property and could activate H_2O_2 to produce effective oxidizing reagent realizing MB discoloration. Heterojunction established in the composite accelerated the process of electron-hole pair separation and boosted H_2O_2 activation and photo-Fenton reaction. As a whole, the uniformity of particle size and morphology still needs improved by adjusting synthesis conditions. The magnetic character of $NiFe_2O_4$ can be introduced to other composite for repeating use photocatalystand enhancingphotodegradation abilitysimultaneously.

Acknowledgements

This work was supported by the National Nature ScienceFoundation of China (21476097, 21407065, 21406094), Natural Science Foundation of Jiangsu Province (No. BK20130513, BK20140533), University Natural Science Research of Jiangsu (No.13KJB430007), Jiangsu Key Lab of Material Tribology Foundation (No.Kjsmcx201303), the Senior Intellectuals Fund of Jiangsu University (No. 12JDG110), Jiangsu University Graduate Student Research and Creative Project (No.KYXX-0012).

Notes and references

[a] *School of Materials Science & Engineering, Jiangsu University, Zhenjiang 212013, P. R. China*
[b] *Institute for Energy Research, School of Chemistry and Chemical Engineering, Jiangsu University, Zhenjiang 212013, P. R. China*
[c] *Hainan Provincial Key Lab of Fine Chemistry, Hainan University, Haikou, Hainan 570228, P.R. China*
***Corresponding author:** Tel.:+86-0511- 88791108; Fax: +86-0511-88791108*
E-mail address: xh@ujs.edu.cn; lihm@ujs.edu.cn

1 X. Chen, H-Y.Zhu, J-C.Zhao, Z-F.Zheng and X-P.Gao, *Angew. Chem. Int. Ed*., 2008, **47**, 5353-5356.
2 A. Kudo and Y. Miseki, *Chem. Soc. Rev*., 2009, **38**, 253-278.
3 G. Vincent, A. Aluculesei, A. Parker, C. Fittschen, O. Zahraa and P-M.Marquaire, *J. Phys. Chem. C*, 2008, **112**, 9115-9119.
4 X. J. She, H. Xu, Y. G. Xu, J. Yan, J. X. Xia, L. Xu, Y. H. Song, Y. Jiang, Q. Zhang and H. M. Li, *J. Mater. Chem. A*, 2014, **2**, 2563-2570.
5 S. H. Sun, H. Zeng, D. B. Robinson, S. Raoux, P. M. Rice, S. X. Wang and G. X. Li, *J. Am. Chem. Soc.*, 2004, **126**, 273-279.
6 U. Lüders, A. Barthélémy, M. Bibes, K. Bouzehouane, S. Fusil, E. Jacquet, J-P.Contour, J-F.Bobo, J. Fontcuberta and A. Fert, *Adv. Mater*., 2006, **18**, 1733-1736.
7 S. Balaji, R. K.Selvan, L. J.Berchmans, S. Angappan, K. Subramanian, C. O. Augustin, *Mater. Sci. Eng., B*, 2005, **119**, 119-124.
8 Q-C. Sun, H. Sims, D. Mazumdar, J. X. Ma, B. S. Holinsworth, K. R. O'Neal, G. Kim, W. H. Butler, A. Gupta and J. L. Musfeldt, *Phys. Rev. B*, 2012, **86**, 205106-205110.
9 M. Meinert and G. Reiss, *J. Phys.: Condens. Matter*, 2014, **26**, 115503-115506.
10 G. Rekhila, Y. Bessekhouad and M. Trari, *Int. J. of Hydrogen Energy*, 2013, **38**, 6335-6343.
11 S. Rana, R.S. Srivastava, M.M. Sorensson and R.D.K. Misra,*Mater. Sci. Eng., B*, 2005, **119**, 144-151.
12 K. N. Harish, H. S. B. Naik, P. N. P. Kumar and R. Viswanath, *ACS Sustainable Chem. Eng.*, 2013, **1**, 1143-1153.
13 P. Xiong, Y. S. Fu, L. J. Wang and X. Wang.*Chem. Eng. J.*, 2012, **195-196**, 149-157.
14 Y. S. Fu, H. Q. Chen, X. Q. Sun and X. Wang, *AlChE J.*, 2012, **58**, 3298-3305.
15 S. Bai, X. J. Wang, C. Y. Hu, M. L. Xie, J. Jiang and Y. J. Xiong, *Chem. Commun.*, 2014, **50**, 6094-6097.
16 Y. Wang, X. C. Wang, and M. Antonietti, *Angew. Chem. Int. Ed*., 2012, **51**, 68-89.
17 X. C. Wang, K. Maeda, A. Thomas, K. Takanabe, G. Xin, J. M. Carlsson, K. Domen and M. Antonietti,*Nat. Mater.*, 2009, **8**, 76-80.
18 Y. L. Tian, B. B. Chang, J. L. Lu, J. Fu, F. N. Xi and X. P. Dong, *ACS Appl. Mater. Interfaces*, 2013, **5**, 7079-7085.
19 H. Katsumata, Y. Tachi, T. Suzuki and S. Kaneco, *RSC Adv.*, 2014, **4**, 21405-21409.
20 L. Y. Huang, H. Xu, Y. P. Li, H. M. Li, X. N. Cheng, J. X. Xia, Y. G. Xu and G. B. Cai, *Dalton Trans.*, 2013, **42**, 8606-8616.
21 W. Liu, M. L. Wang, C. X. Xu and S. F. Chen.*Chem. Eng. J.*, 2012, **209**, 386-393.
22. C. S. Pan, J. Xu, Y. J. Wang, D. Li and Y. F. Zhu. *Adv. Funct. Mater.*, 2012, **22**, 1518-1524.
23 N. Tian, H. W. Huang, Y. He, Y. X. Guo, T. R. Zhang and Y. H. Zhang.*Dalton Trans.*, 2015.**44**, 4297-4307.
24 J. Y. Zhang, Y. H. Wang, J. Jin, J. Zhang, Z. Lin, F. Huang and J. G. Yu, *ACS Appl. Mater. Interfaces*, 2013, **5**, 10317-10324.
25 F. Chang, Y. C. Xie, J. Zhang, J. Chen, C. L. Li, J. Wang, J. R Luo, B. Q. Deng and X. F. Hu, *RSC Adv.*, 2014, **4**, 28519-28528.
26 Z. W. Zhao, Y. J. Sun and F. Dong, *Nanoscale*, 2015, **7**, 15-37.
27 J. Chen, S. H. Shen, P. H. Guo, P. Wu and L. J. Guo, *J. Mater. Chem. A*, 2014, **2**, 4605-4612.
28 S. W. Zhang, J. X. Li, M. Y. Zeng, G. X. Zhao, J. Z. Xu, W. P. Hu and X. K. Wang, *ACS Appl. Mater. Interfaces*, 2013, **5**, 12735-12743.
29 Y. J. Yao, Y. M. Cai, F. Lu, J. C. Qin, F. Y. Wei, C. Xu and S. B. Wang, *Ind. Eng. Chem. Res.*, 2014, **53**, 17294-17302.
30 H. Zhang, R. L. Zong, J. C. Zhao and Y. F. Zhu, *Environ. Sci. Technol.*, 2008, **42**, 3803-3807.
31 T. Zhou, Y. G. Xu, H. Xu, H. F. Wang, Z. L. Da, S. Q. Huang, H. Y. Ji and H. M. Li, *Ceram. Int.*, 2014, **40**, 9293-9301.
32 H. Xu, J. Yan, Y. G. Xu, Y. H. Song, H. M. Li, J. X. Xia, C. J. Huang and H. L. Wan, *Appl. Catal., B*, 2013, **129**, 182-193.
33 S. Diodati, L. Pandolfo, A. Caneschi, S. Gialanella and S. Gross, *Nano Res.*, 2014, **7**, 1027-1042.
34 M. M. Bućko and K. Haberko, *J. Eur. Ceram. Soc.*, 2007, **27**, 723-727.
35 Q. J. Xiang, J. G. Yu and M. Jaroniec, *J. Phys. Chem. C*, 2011, **115**, 7355-7363
36 Y. J. Wang, R. Shi, J. Lin and Y. F. Zhu, *Energy Environ. Sci.*, 2011, **4**, 2922-2929.
37 K. B. Modi, S. J. Shah, N. B. Pujara, T. K. Pathak, N. H. Vasoya and I. G. Jhala, *J. Mol. Struct.*, 2013, **1049**, 250-262.
38 J. L. Gunjakar, A. M. More, K. V. Gurav and C. D. Lokhande, *Appl. Surf. Sci.*, 2008, **254**, 5844-5848.
39 V. K. Mittal, P. Chandramohan, S. Bera, M. P. Srinivasan, S. Velmurugan and S. V. Narasimhan, *Solid State Commun.*, 2006, **137**, 6-10.
40 S. Bera, A. A. M. Prince, S. Velmurugan, P. S. Raghavan, R. Gopalan, G. Panneerselvam, S. V. Narasimhan, *J. Mater. Sci.*, 2001, **36**, 5379-5384.
41 A. Thomas, A. Fischer, F. Goettmann, M. Antonietti, J. O. Müller, R. Schlögl and J. M. Carlsson,*J. Mater. Chem.*, 2008, **18**, 4893-4908.
42 L. Ge, C. C. Han, X. L. Xiao and L. L. Guo,*Appl. Catal., B*, 2013, **142-143**, 414-422.
43 Y. F. Liu, W. Q. Yao, D. Liu, R. L. Zong, M. Zhang, X. G. Ma and Y. F. Zhu, *Appl. Catal., B*, 2015, **163**, 547-553.
44 L.Q. Ye, J.N. Chen, L.H. Tian, J.Y. Liu, T.Y. Peng, K.J. Deng and L. Zan, *Appl. Catal. B*, 2013, **130-131**, 1-7.
45 H.F. Cheng, B.B. Huang, Y. Dai, X.Y. Qin and X.Y. Zhang, *Langmuir*, 2010, **26**, 6618-6624.
46 P. F. Zhang, Y. T. Gong, H. R. Li, Z. R. Chen and Y. Wang, *RSC Adv.,* 2013, **3**, 5121-5126.
47 P. F. Zhang, Y. Wang, H. R. Li and M. Antonietti, *Green Chem.,* 2012, **14**, 1904-1908.
48 P. F. Zhang, Y. Wang, J. Yao, C. M. Wang, C. Yan, M. Antonietti and H. R. Li, *Adv. Synth. Catal.,* 2011, **353**, 1447-1451.
49 R. Sharma, S.Bansal and S. Singhal, *RSC Adv.*, 2015, **5**, 6006-6018.

